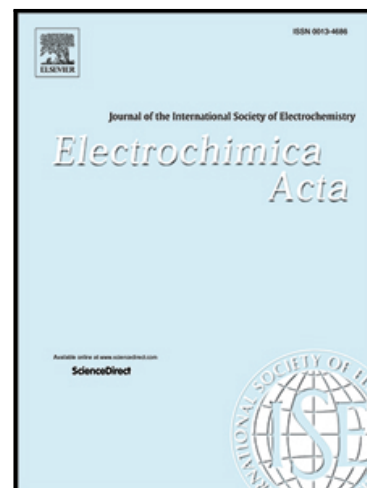# Journal Pre-proof

Electrochemical Stability of Metal Nanoparticles: the role of Size-Distribution Broadness

Leonardo D. Robledo Candia , Gabriel C. Lavorato ,
Aldo A. Rubert , Mariano H. Fonticelli

Please cite this article as: Leonardo D. Robledo Candia , Gabriel C. Lavorato , Aldo A. Rubert , Mariano H. Fonticelli , Electrochemical Stability of Metal Nanoparticles: the role of Size-Distribution Broadness, *Electrochimica Acta* (2023), doi: https://doi.org/10.1016/j.electacta.2023.143546

Highlights

- The electrochemical stability of metal nanoparticles depends on their average size.

- The broadness of the size distribution determines the nanoparticles' stability.

- Nernstian behavior is expected regardless of the size distribution shape.

- The mixed potential theory predicts the metal nanoparticles' stability.

- Charge transfer is a bottleneck in Electrochemical Ostwald Ripening.

Highlights

Electrochemical Stability of Metal Nanoparticles: the role of Size-Distribution Broadness

Leonardo D. Robledo Candia, Gabriel, C. Lavorato, Aldo A. Rubert, Mariano H.

Fonticelli[,*]

Instituto de Investigaciones Fisicoquímicas, Teóricas y Aplicadas
Universidad Nacional de La Plata- CONICET, Argentina. Diagonal 113 y 64 S/N
(1900) La Plata, Buenos Aires
* Corresponding author: Mariano H. Fonticelli
Fax: (+54) 221425 4642
Phone: (+54) 221425 7430
E-mail: mfonti@inifta.unlp.edu.ar

ABSTRACT: In this article, we develop a thermodynamic and an electrochemical kinetic model to study the stability of metal nanoparticles (MNPs) supported on an inert substrate and in contact with an electrolyte. Regardless of the model, we find that the redox potential is a property of the entire MNPs' size distribution, which has to be characterized by, at least, its mean and variance. The thermodynamic model, which considers only the excess free energy due to the increased surface-to-volume ratio on MNPs, predicts an increase in surface effects as the size distribution becomes broader. On the other hand, the electrochemical kinetic approach models the MNPs as reactive systems considering the changes in the heterogeneous-rate constants due to surface effects. This allows the use of the mixed potential theory to evaluate the electrode potential, which would be experimentally accessible, showing a tendency contrary to that predicted by the thermodynamic model for closed systems. Then, the electrochemical boundary conditions –i.e., charge conservation- have to be considered rather than just the thermodynamic criteria. Also, it is analyzed under which circumstances the charge-transfer processes control the electrode potential, instead of mass-transfer. Hence, it is shown that the electrochemical kinetic approach

is applicable to the study of the electrochemical Ostwald ripening among many other processes.

Keywords: nanoparticles' stability, mixed potential theory, thermodynamic approach, size-distribution broadness, charge-transfer control.

1.-Introduction

Metal nanoparticles (MNPs) are of great importance for diverse fields such as electronics, sensing, catalysis, medicine, and energy storage, among others, due to their non-conventional physical and chemical properties [1–5]. However, stability against oxidation is critical for metal nanostructures to retain their distinguishing properties [6–9], since metal dissolution changes both the size and shape of the MNPs. For this reason, several groups used electrochemical techniques and microscopy tools to study the size-dependent oxidation potential of MNPs [10–14]. However, the widely used stripping analysis [12,15–17] can lead to a bias in the derivation of the thermodynamic quantities, since the MNPs' size considerably changes throughout the potential sweep. Although Neuman et al. [17] have theoretically analyzed the change in the formal potential when the size of the MNPs changes due to the potential scanning, the width of the size distribution could represent a serious drawback in the data analysis. In this regard, the analysis presented in this paper would help to clarify the effect of size distribution. On the other hand, recent studies have dealt with MNPs' stability by means of electromotive forces measurements [18–22]. Besides the many drawbacks inherent to the experimental approaches to study the MNPs' stability, theoretical methods have not been adequately developed to account for the important effects that the size distribution broadness has on the thermodynamic parameters.

Early work [23] has dealt with thermodynamic approaches that took into account the enhanced tendency to oxidation that MNPs have due to its excess surface energy.

3

Within the context of the Gibbs-Thompson equation, which represents the simplest approach to this problem, the excess of chemical potential for monodisperse MNPs ($\Delta\mu_{mono}$) raises due to the increase in the surface to volume ratio. Since for monodisperse systems the size of any particle coincides with the mean size, the MNPs' stability has been described for spherical particles on the basis of their electrode potential, E_{M^{z+}/M^0}^{NP}, as a function of the mean diameter, $\bar{d}$. Therefore, according to the seminal work by W. J. Plieth [23]:

$$E_{M^{z+}/M^0}^{NP} = E_{M^{z+}/M^0}^{Bulk} - \frac{\Delta\mu_{mono}}{zF}, \quad \Delta\mu_{mono} = \mu^{NPs} - \mu^{Bulk} = \frac{4\gamma V_m}{\bar{d}} \qquad [1]$$

where γ, F and V_m are the specific surface free energy, Faraday's constant and the molar volume of the bulk metal, respectively. E_{M^{z+}/M^0}^{Bulk} is the electrode potential of the bulk metal, which depends on the M^{z+} activity ($a_{M^{z+}}$) and can be calculated using the Nernst equation.

In this work, we develop simple models that emphasize concepts and phenomena that have not been considered in previous studies. Therefore, we just consider differential contributions of the form γdA to the free energy of the system. The differences among the γ values for the distinct faces exposed by non-spherical particles and other kinds of surface effects are not considered, although this is not generally a realistic assumption. Also, we restrict our study to metal particles large enough so they don't exhibit quantum confinement effects (>2-3 nm) [17,24,25]. We don't consider in this paper further details in the description of surface stress and tension for solid metal electrodes. For comprehensive discussions on these topics see the works by Schmickler et al. [26] and Lipkowski et al. [27]. Since these details are not at the main focus of our study, we highlighted the relevant factors by means of simple models. Indeed, recent reports interpret the electrochemical properties according to the model by Plieth [4,9,19,21,28–31]. We anticipate that the electrochemical kinetic model developed here could be

extended by taking into consideration other contributions to the chemical potential of the MNPs; for instance, the electrostatic energy due to the net charge onto the MNPs [32,33], and those mentioned above. However, because surface tension depends on charge density [26,34], an accurate model should consider the interrelationship between these quantities.

Most of the previous studies have modeled ensembles of MNPs as if they were monodisperse systems. However, real samples of MNPs are polydisperse. This type of systems imposes challenges in characterizing them through observable macroscopic variables. In this regard, great advances have been made in the description of magnetic systems [35]. For example, Wang Xu-Fie et al. [36] analyzed the effect of polydispersity of magnetic nanoparticles on their saturation magnetization, which depends, not only in the mean size, but on the standard deviation of the size distribution. However, chemical reacting systems present additional complications, especially in the definition of intensive variables[37–39]. In particular, the definition of the redox potential of a polydisperse ensemble of MNPs on an inert electrode is not trivial. This is mainly because the different tendencies of the MNPs towards oxidation and reduction. In section 2.1 we tackle this problem by showing that the redox potential would be experimentally accessible, i.e., it is an operationally defined variable.

Few studies have dealt with the effect of polydispersity on the electrochemical properties of MNPs [40,41]. Brainina et al. [41] analyzed this feature on the electrooxidation of MNPs, by considering the excess free energy in terms of the ratio between the average area per particle and the average number of atoms per particle. This is, the ratio between the second and the third moments of the size distribution, respectively. Nevertheless, this excess free energy does not converge to that predicted by the Gibbs-Thomson equation when the distribution becomes monodisperse.

On the other hand, in the thermodynamic approach proposed by T. Hill [39] the excess chemical potential for an ensemble of polydisperse unreactive particles ($\Delta\mu_{poly}$) depends on -at least- two statistical parameters, i.e., the mean size and variance. Within Hill's model each particle in the ensemble is considered as a closed system. It might be expected that some properties of MNPs would not depend strongly on their reactivity or, more precisely, on the rate of the reactions that occur on their surfaces. Instead, the rate of electrochemical reactions is closely related to the electrode potential. Therefore, it would be expected that the redox potential is determined by the reactions experienced by the ensemble of nanoparticles. Then, a model based on electrochemical kinetics concepts would be useful to describe these systems. Indeed, Schröder et al. [40] proposed a model that uses concepts from the theory of mixed potentials [42] and a linearized version of the Butler-Volmer equation to estimate the potential of a set of polydisperse MNPs on an inert electrode. However, we will show that this model is not suitable for real dispersions of small MNPs because the conditions for the use of the linearized Butler-Volmer equation are not correct for systems that contain particles smaller than approximately 10 nm.

In this paper we address the question posed by Plieth [23], "What is the redox potential of MNPs in a dispersed state?", taking into consideration different fundamental aspects. First, we considered the redox potential as an operational variable, demonstrating that it would be accessible through open circuit potential, *ocp*, measurements (Section 2.1). Then, we took advantage of the model developed by Hill, Chapter 13 in Ref. [39], which provides $\Delta\mu_{poly}$ in terms of mean size and variance, to analyze how the redox potential would depend on these statistical variables if this purely thermodynamic approach was appropriate.

Afterwards, in Section 2.2, we present a model based on electrochemical kinetics, which circumvents the restriction of considering the MNPs as closed (unreactive) entities. Our approach, which is based on the theory of mixed potentials [42] is relevant to many systems of interest in applications. We also show that, on a wide variety of practically useful conditions, the reactions are controlled by charge transfer processes. This demonstrates that the electrochemical systems require alternative descriptions, different from those widely discussed in nucleation and growth models, which are usually controlled by mass transfer (see, for instance, Chapter 16, section 7.6 in Ref. [43]). Moreover, it should be noted that our results are applicable whatever is the size-distribution (for instance, Gaussian, log-normal, etc.). Therefore, the electrochemical kinetic model developed in this work is more suitable for studying processes such as electrochemical Ostwald ripening in a wider range of conditions than those addressed in previous works. In section 3, "Results and Discussion", we analyze the chemical, electrostatic and surface contributions to E for a monodisperse system (Section 3.1). Then, we quantitatively evaluate the effect of a reduced size and the distribution broadness on E; and we also discuss the applicability of our thermodynamic approach to describe actual ensembles of supported MNPs (Section 3.2). In section 3.3 we present the limiting case of ensembles of MNPs large enough to be described by the linearized Butler-Volmer equation. Also, in this case we show that a proper evaluation of E requires knowing both the average size and its variance. Afterwards, we apply the electrochemical model to different size distributions that mimic actual MNPs ensembles (Section 3.4); i.e., those with considerably high broadness. We found that even for relatively narrow size-distributions most of the current comes from MNPs that must be described by the full Butler-Volmer equation. In section 3.5 we compare both approximations by considering a limited set of size distributions (narrow, Gaussian distributions), since the

thermodynamic approach is more restrictive than the electrochemical one. Throughout the comparison of the results from both approximations, we found opposite behaviors. While the thermodynamic approach predicts an enhancement of the surface effect due to the increase in size broadness, the electrochemical kinetic model shows an attenuated outcome. Finally, we provide further arguments in favor of the electrochemical model.

2.- Theoretical Models
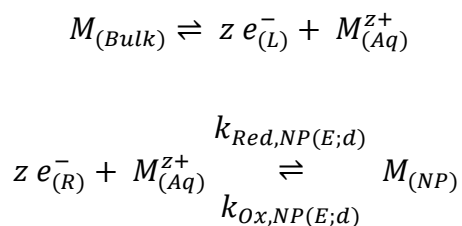
2.1 Thermodynamic Approach

2.1.1 Measurability of the Electrode Potential

First, we will discuss whether the electrode potential due to an ensemble of MNPs onto an inert substrate can be defined as a measurable quantity. Indeed, the definition of a thermodynamic quantity is supposed to have a definite operational meaning in terms of measurable quantities [44,45]. To do so, we analyze an electrochemical cell whose net effect is the formation of an ensemble of MNPs from the bulk metal (Scheme 1).

The cell consists of two electrodes: the left one (L), which can be seen as a reference electrode, is made of the bulk metal (M); while the right one (R) consists of an inert conducting material (S) that supports the ensemble of NPs constituted from the same metal. In short, the cell in Scheme 1 can be briefly described as follows:

$$M^L \, / \, M^{z+}(a_{M^{z+}}) \, / \, M_{(NP)}/ \, S \, / \, M^R$$
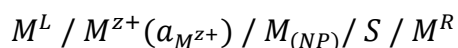
Note that both terminals are made of the same metal. Formally, the half reactions at the left and right electrodes are, respectively,

$$M_{(Bulk)} \rightleftharpoons z \, e^-_{(L)} + \, M^{z+}_{(Aq)}$$

$$z \, e^-_{(R)} + \, M^{z+}_{(Aq)} \; \underset{k_{Ox,NP(E;d)}}{\overset{k_{Red,NP(E;d)}}{\rightleftharpoons}} \; M_{(NP)}$$

The electrolyte contains metallic species (for simplicity, aqueous cations $M_{(Aq)}^{z+}$), with activity $a_{M^{z+}}$. The cell potential, E, is the difference between the Galvani potentials
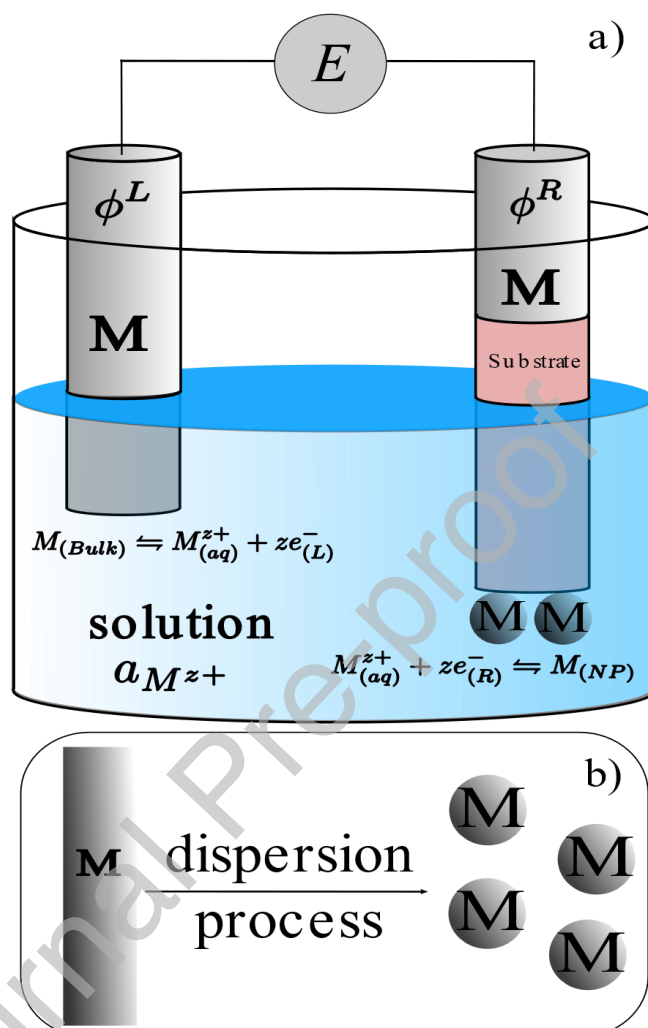
Scheme 1. (a) Arrangement for the measurement of the redox potential of supported MNPs. (b) Schematic representation of the dispersion of metal *M*.

of the right side (ϕ^R) and the left side (ϕ^L) electrodes. Since the net effect of the cell operation is the dispersion of the metal (Scheme 1, panel b), the reaction is expected to be non-spontaneous, so $E < 0$ [23].

Following the standard reasoning, which consist in the analysis of every potential difference throughout the electrochemical cell and equating the electrochemical potential of the electrons between conducting faces in contact [46], we found (see Supporting Information, SI):

$$(\phi^R - \phi^L) = \left[\Delta^{NP}\phi^{Sol} - \frac{\mu_e^{NP}}{F}\right] - \left[\Delta^L\phi^{sol} - \frac{\mu_e^M}{F}\right] \qquad [2]$$

where μ_e^{NP} and μ_e^M are the chemical potentials of the electrons in the MNPs and the bulk metal, respectively; $\Delta^{NP}\phi^{Sol}$ is the Galvani potential differences between the MNPs and the solution and $\Delta^L\phi^{Sol}$ is the potential difference between the left electrode and the solution. Eq.2 express the measured potential, $E = (\phi^R - \phi^L)$, in terms of the absolute potentials of the MNPs/solution and M/solution electrodes: $E_{abs}^{NP} = \left[\Delta^{NP}\phi^{Sol} - \frac{\mu_e^{NP}}{F}\right]$ and $E_{abs}^M = \left[\Delta^L\phi^{sol} - \frac{\mu_e^M}{F}\right]$ [46]:

$$E = E_{abs}^{NP} - E_{abs}^M \qquad [3]$$

Therefore, it can be seen that the experimentally accessible quantity E has both an electrostatic and a chemical contribution, since in general the chemical potential of the electrons differs from one material to another. After introducing the corresponding equilibrium conditions in terms of the electrochemical potentials of reacting species (see SI), E can be expressed by means of the difference ($\Delta\mu$) between the chemical potential of M in the MNPs and that on the bulk metal: $\Delta\mu = \mu_M^{NP} - \mu_M^{Bulk}$.

$$E = (\phi^R - \phi^L) = -\frac{\Delta\mu}{zF} \qquad [4]$$

Note that $\Delta\mu$ is the excess chemical potential due to the MNPs' formation process from the bulk metal, which is the net transformation due to the cell reaction. Indeed, the cell potential would be zero for particles of macroscopic size. Therefore, it is clear from Eq. 3 that the redox potential of polydisperse ensembles of MNPs would be experimentally accessible through *ocp* measurements of this cell. According to Eq. 4, the prediction of the redox potential would require the knowledge of $\Delta\mu$ for the particular set

of particles. This issue is treated in the following on a purely thermodynamic basis by following the formalism proposed by Hill in Ref. [39], Chapter 13.

2.1.2 The Chemical Potential of a Polydisperse Ensemble of Nanoparticles

Consider an ensemble of closed small systems (Chapter 13, in Ref. [39]). The ensemble as a whole is characterized by their temperature (T) and pressure (p). Additionally, every small system is characterized by the size of the only particle in it, i.e., the number of atoms N, of the particle. Although considering closed systems, we are interested in the effects of varying N. Thus, a polydisperse sample made of an ensemble of closed systems of varying N will be studied. The average Gibbs free energy of a single particle in the ensemble is:

$$G = \sum_N G_N P_N \qquad [5]$$

where P_N is the fraction of particles in the ensemble with size N and G_N is the Gibbs free energy of a single N-sized particle. Following Hill, we arbitrarily choose a Gaussian distribution defined by two parameters the mean value, $\overline{N}$, and the standard deviation, σ_N, of N. This choice, which represents a relatively strong limitation, is necessary since this model can only be applied to size-distributions that have a mean mathematically independent of the dispersion parameter (see Eq. 16-6, page 173 in Ref. [39]). In contrast, for the log-normal distribution, which is usually used to describe size distributions [47], the mean and the standard deviation are mutually dependent since both depend on the median and the geometric standard deviation (see SI, and Ref. [47], Chapter 2, Section 2.3). After expressing the volume of a single particle (V) as $V = N\nu$ (where ν is the volume per atom), taking into consideration the surface free energies contribution by

means of the Gibbs-Thompson equation and considering spherical particles, the expression for G_N ($G_N = G_N^{Bulk} + \gamma A$) becomes:

$$G_N = N\left(\mu_M^{Bulk}/N_{Av}\right) + 6^{2/3}\pi^{1/3}\gamma v^{2/3}N^{2/3} \qquad [6]$$

where N_{Av} is the Avogadro's number.

Equations 5 and 6 allow the derivation of the chemical potential for a polydisperse ensemble of MNPs, $\mu_{(T,p,\bar{N},\sigma_N)}$. The following expression is valid for narrow Gaussian distributions, which only has significative contributions to G_N for N values close to $\bar{N}$ (see SI for further details):

$$\begin{aligned}
\mu_{(T,p,\bar{N},\sigma_N)} = &\mu_M^{Bulk} \\
&+ \frac{2}{3}6^{2/3}\pi^{1/3}\gamma v^{2/3}\bar{N}^{-1/3}\left[1 + \frac{2}{9}\left(\frac{\sigma_N}{\bar{N}}\right)^2 + \frac{35}{81}\left(\frac{\sigma_N}{\bar{N}}\right)^4\right. \\
&\left.+ \cdots\right]N_{Av}
\end{aligned} \qquad [7]$$

Then, we can express the redox potential according to Eq. 8:

$$\begin{aligned}
E = &E_{M^{z+}/M^0}^{Bulk} - \frac{\left(\mu_{(T,p,\bar{N},\sigma)} - \mu_M^{Bulk}\right)}{zF} \\
= &E_{M^{z+}/M^0}^{Bulk} \\
&- \frac{26^{2/3}\pi^{1/3}\gamma v^{2/3}N_{Av}\bar{N}^{-1/3}}{3zF}\left[1 + \frac{2}{9}\left(\frac{\sigma_N}{\bar{N}}\right)^2 + \frac{35}{81}\left(\frac{\sigma_N}{\bar{N}}\right)^4\right. \\
&\left.+ \cdots\right] = E_{rev}^{Bulk} - \frac{\Delta\mu_{poly(T,p,\bar{N},\sigma_N)}}{zF}
\end{aligned} \qquad [8]$$

Note that: (i) as $\Delta\mu_{poly} = \mu_{(T,p,\bar{N},\sigma)} - \mu_M^{Bulk}$ is the chemical potential increase due to the dispersion process, E depends on both $\bar{N}$ and σ_N (ii) E should show Nernstian behavior since E_{M^{z+}/M^0}^{Bulk} is the only term which depends on the cations' activity, and (iii) for very large average sizes $E \to E_{M^{z+}/M^0}^{Bulk}$. The last equation would be applicable to an ensemble of MNPs with a narrow Gaussian distribution if they behave as unreactive entities. Instead, to deal with the fact that electrochemically active metals are not inert, in the next section we will present an alternative approach based in concepts of electrochemical

kinetics. Nonetheless, it is important to note that according to Eq. 8, for a fixed $\bar{N}$, the surface free energy contribution would be increasingly relevant as the distribution becomes wider.

2.2 Electrochemical Kinetic Approach

In this section we present an alternative approach to predict the electrode potential of an array of polydisperse MNPs onto an inert electrode, which is based on electrochemical kinetics. Our model considers that Ostwald ripening by surface diffusion has a negligible contribution in comparison with electrochemical Ostwald ripening [48], and that the transfer reaction $z\,e_{(R)}^{-} + M_{(Aq)}^{z+} \rightleftharpoons M_{(NP)}$ is the slowest process. Therefore, we first describe how the increased surface energy of the MNPs affects the specific rate constants of the oxidation and reduction processes. Then, we support the idea that charge transfer processes determine the behavior of MNPs under the usual conditions for the occurrence of the electrochemical Ostwald ripening. Instead, mass transport phenomena have also to be considered in stripping essays [17], since a large departure from equilibrium is imposed during the potential sweep. Finally, we apply the mixed potential theory to find an explicit expression of the electrode potential. One of the main conclusions of this section is that our model predicts a Nernstian behavior, regardless of the shape of size distribution, even though MNPs are reacting out-of-equilibrium entities.

The electrochemical reaction on the right electrode of Scheme 1 has associated their corresponding forward and backward rate constants, $k_{Red,NP(E;d)}$ and $k_{Ox,NP(E;d)}$, respectively. We expect that both rate constants would depend on the size of the MNP, since the chemical potential of the metal depends on it [49–51], for this reason their dependence with d are explicitly written. Moreover, a fraction α of the excess chemical potential, $\Delta\mu_{(d)}$, for the particles having size d promotes the activated oxidation while a complementary quantity $(1-\alpha)\,\Delta\mu_{(d)}$ retards the reduction. For simplicity we assign α

13

a meaning equivalent to what is usually given to the transfer coefficient (See details in the SI):

$$k_{Ox,NP(E;d)} = k_{Ox,bulk(E)} exp[\alpha\Delta\mu_{(d)}/RT]$$
$$k_{Red,NP(E;d)} = k_{Red,bulk(E)} exp[-(1-\alpha)\Delta\mu_{(d)}/RT]$$

[9]

It should be noted that the rate constants depend on the electrode potential and, parametrically, on the size of the nanoparticles. Although a plausible choice is to take the potential of the $E^{Bulk}_{M^{z+}/M^0}$ as the reference potential, we will write it down explicitly to emphasize its role in our conclusions. On the other hand, the dependence on d is not restricted to systems that obey the Gibbs-Thompson equation. Furthermore, Equation 1 could be formulated to account for other contributions, such as the dependence of interfacial tension on NPs' size [22], surface stress [26,27], and/or to weight the different free energies of crystal faces by means of the Wulf's rule [51], as has already been applied to model the electrochemical behavior of metallic NPs [51,53]. For example, Kuo and Hwang demonstrated that morphology, structural defects, and facet surface energy strongly affect the electrochemical oxidation potentials of metallic NPs [54]. Moreover, other contributions to μ^{NPs}, as that from the electrostatic energy [32], can be added to $\Delta\mu$, which easily extends the applicability of the present model.

Following the same procedure usually employed in electrochemistry textbooks [34] we used the expressions of the rate constants to derive the Butler-Volmer equation for a single particle (see SI):

$$j_{NP(E;d)} = j_0 \left\{ e^{\alpha f(E-E_{(d)})} - \frac{C^{surf}_{M^{z+}}}{C^*_{M^{z+}}} e^{-(1-\alpha)f(E-E_{(d)})} \right\}$$

[10]

$j_{NP(E;d)}$ is the current density of a single particle of size d when E is the applied potential; since the dependence with d is within $E_{(d)}$, j_0 is the exchange current density of the bulk

metal. $C_{M^{z+}}^{surf}$ and $C_{M^{z+}}^{*}$ are the surface and bulk concentrations of M^{z+}, respectively; $E_{(d)} = E_{M^{z+}/M^0}^{Bulk} - \Delta\mu_{(d)}/zF$ and $f = zF/RT$. The quotient $C_{M^{z+}}^{surf}/C_{M^{z+}}^{*}$ can be written in terms of $j_{NP(E;d)}$ and the limiting diffusional current density, $j_{L(d)}$ [55,56], leading to:

$$j_{NP(E;d)} = j_0 \left\{ e^{\alpha f\left(E - E_{(d)}\right)} - \left[1 - \frac{j_{NP(E;d)}}{j_{L(d)}}\right] e^{-(1-\alpha)f\left(E - E_{(d)}\right)} \right\} \qquad [11]$$

The high fluxes of matter and the plausible predominance of charge transfer have been widely considered for ultramicroelectrodes[34,56,57]. Therefore, for MNPs with a size of a few tens of nanometers, Eq.11 reduces to (See SI):

$$j_{NP(E;d)} = j_0 \left\{ e^{\alpha f\left(E - E_{(d)}\right)} - e^{-(1-\alpha)f\left(E - E_{(d)}\right)} \right\} \qquad [12]$$

This equation has the useful form of the Butler-Volmer equation, but it is noticeable that the equilibrium potential of any nanoparticle depends on its size.

Now, we employ Eq.12 to apply the mixed potential theory to the MNPs' array. The null current condition was expressed in terms of the net current over each particle, k, as the product of its area, A_k, and its current density, j_k [42]:

$$0 = \sum_{k=1}^{M} A_k j_{k(E;d_k)} \qquad [13]$$

Where the sum runs over the entire set of MNPs. The choice of the bulk electrode as a reference electrode allows to use E in Eqs. 12 and 13, since for macroscopic particles $E = E_{M^{z+}/M^0}^{Bulk}$ and the current goes to zero. The same reasoning would be appropriate if we had chosen $\Delta^{NP}\phi^{Sol}$ instead of E in Eqs. 10-14, since $\Delta^{NP}\phi^{Sol} \rightarrow \Delta^{L}\phi^{sol}$ and $\frac{\mu_e^{NP}}{F} \rightarrow \frac{\mu_e^{M}}{F}$ for big particles (Eq. 2). Then, the *ocp*, which is a measurable quantity associated with

the mixed potential, $E = E_{mix(\bar{d},\sigma)}$, can be derived from the mixed potential theory (see SI):

$$E_{mix(\bar{d},\sigma)} = E_{M^{z+}/M^0}^{bulk} - \frac{RT}{zF} ln \left(\frac{\sum_k A_k e^{\alpha\frac{\Delta\mu}{RT}}}{\sum_k A_k e^{-(1-\alpha)\frac{\Delta\mu}{RT}}} \right) \qquad [14]$$

It is notable that $E_{mix(\bar{d},\sigma)}$ shows a Nernstian behavior, since E_{M^{z+}/M^0}^{bulk} does, and is the only term that depends on the cations' activity. It has to be remarked that Eq. 14 is a general result, since it does not depend on the particular model chosen to describe $\Delta\mu_{(d)}$, nor on the form of the size distribution.

3. Results and Discussion

3.1. Thermodynamic Analysis of the Cell Potential for Monodisperse Ensembles of Nanoparticles

In this section we analyze the contributions to E for a monodisperse system, in order to highlight some results that are independent of the size-distribution broadness. First, we consider the right-hand electrode, R, in Scheme 1. In equilibrium, the electrochemical potential of the electrons on the MNPs ($\tilde{\mu}_e^{NP}$), the substrate ($\tilde{\mu}_e^{Supp}$), and the right terminal made of M ($\tilde{\mu}_e^R$) have the same value: $\tilde{\mu}_e^R = \tilde{\mu}_e^{NP} = \tilde{\mu}_e^{Supp}$ (Figure 1.a). We will analyze the first equality taking into consideration that, for each phase β, $\tilde{\mu}_e^{\beta} = \mu_e^{\beta} - F\phi^{\beta}$. Furthermore, the electrochemical potential of an electron in a metal is its Fermi energy [46], and the work function, Φ, is defined in terms of electrons in the Fermi level for a metal of zero surface charge. Thus, it is related with μ_e and the surface potential, χ according to: $\Phi = -\mu_e + F\chi$. Note that Φ and μ_e have J/mol as their units. On the other hand, the Galvani potential is the sum of the Volta and surface potentials: $\phi = \psi + \chi$. Thus, we can express $-\tilde{\mu}_e^{\beta} = \Phi^{\beta} + F\psi^{\beta}$, a sum of a chemical and an electrostatic

quantity [46]. From $\tilde{\mu}_e^R = \tilde{\mu}_e^{NP}$ it follows that $\psi^{NP} - \psi^R = -(\Phi^{NP} - \Phi^M)/F$. According to previous studies $\Phi^{NP} > \Phi^M$ [58–60], which implies that $\psi^{NP} < \psi^R$. Since the Volta potential is related to the real charges [61], the last inequality shows that the MNPs will accumulate extra negative charge due to the increase in their work function. Thus, the work function difference is compensated by $-\psi^{NP}F$, which guarantee $\tilde{\mu}_e^R = \tilde{\mu}_e^{NP}$ as shown in Figure 1.a. Next, we can see that the surface effects lead to a further increase in the negative charge of the MNPs, when compared with the right electrode. To do that, we rearrange Eqs. 2 and 4 to find: $E = -\frac{\Delta\mu_{mono}}{zF} = \left[\phi^{NP} - \frac{\mu_e^{NP}}{F}\right] - \left[\phi^L - \frac{\mu_e^M}{F}\right]$. It can be seen that the excess chemical potential due to the metal dispersion is related with an

electrostatic contribution, $[\phi^{NP} - \phi^L]$, as well as a chemical one, $-\frac{1}{F}[\mu_e^{NP} - \mu_e^M]$.

Therefore, the previous expressions of E can be rearranged leading to [62]:

$$-\frac{\Delta\mu_{mono}}{zF} = \frac{(\Phi^{NP} - \Phi^M)}{F} + (\psi^{NP} - \psi^L) \qquad [15]$$

The dispersion process implies $\Delta\mu_{mono} > 0$. Then, the absolute value of the electrical contribution, $|\psi^{NP} - \psi^L|$, results larger than the chemical one: $|\psi^{NP} - \psi^L| > (\Phi^{NP} - \Phi^M)/F$.
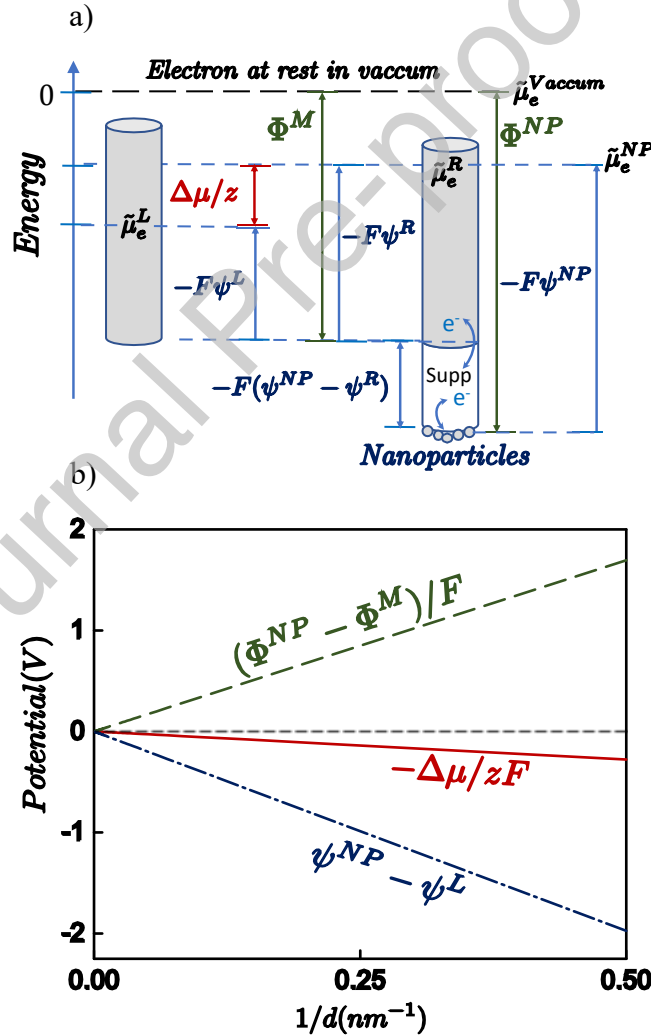

Figure 1. (a) Electrochemical potential (energy) diagram of the electrons in the cell of Scheme 1. (b) Representation of the contributions in Eq. 15 for silver nanoparticles ($\gamma = 1.3\ Jm^{-2}$, $\rho = 10490\ kgm^{-3}$) with sizes between 2 to 100 nm.

18

Now, we analyze in some detail the expected magnitudes for the aforementioned contributions. Briefly, we take advantage of the in-depth studies on the variation of work function with size to roughly calculate $\Phi^{NP} - \Phi^{M}$. In addition, we apply the Gibbs-Thompson equation to approximate $\Delta\mu_{mono}$. Thus, we are able to estimate $\psi^{NP} - \psi^{L}$. Although there is no experimental consensus on how Φ varies with size, classical and quantum-based models predict an increase in the work function as the diameter of spherical particles decreases [58]. This behavior has been verified on a variety of real systems, as naked [59] and citrate-covered nanoparticles [63], although the opposite trend has been also reported, which could be related to charge transfer between the ligands and the metallic core [64]. Φ can be expressed as a linear function of d^{-1} when an electrostatic approach, which takes into consideration the image forces, is applied [59]:

$$\Phi_{(d)}^{e} = \Phi^{M} + \frac{C_{p}e^{2}}{2\pi\varepsilon_{0}d}N_{Av} \quad (for\ C_{P} = 3/8) \qquad [16]$$

The superscript "e" stresses the fact that $\Phi_{(d)}^{e}$ is estimated by means of an electrostatic model, and Φ^{M} corresponds to the bulk material. Then, we can use the approximation $(\Phi^{NP} - \Phi^{M})/F = \frac{C_{p}e^{2}}{2\pi\varepsilon_{0}d}\frac{N_{Av}}{F}$, which is represented in Figure 1.b as function of the reciprocal of size, d^{-1} (dark-green line). It can be observed that the contribution from the work function difference is positive and quite large. Also, Figure 1.b shows the contribution from the excess of chemical potential -the left side of Eq. 15- for Ag nanoparticles, Ag NPs, as a model-system [17] according to the Gibbs-Thompson equation (dark-red trace). The choice of the γ for bulk Ag [17] results in a small contribution from the surface work, in comparison to that related to the work function. Although we could have considered the dependence of γ with size [4], this would not lead to qualitatively different results. Therefore, here and in the following we will attach to the

simplest model. On the other hand, the Volta potential difference is negative and quite important: about -1 V, for MNPs of 4 nm (blue line in Figure 1.b). Notably, the surface energy contribution to E is negative and comparatively smaller. Thus, most of the $\psi^{NP} - \psi^L$ compensates the huge variation in work function difference, which is related to $\psi^{NP} - \psi^R$, while the remaining balances the surface excess contribution. Our analysis shows that the large change in the work function and the relatively small contribution from surface work due to dispersion process leads to the development of considerable Volta potential difference. On the other hand, the previous reasoning does not allow us to know the Galvani potential difference between the MNPs and the massive electrode: $[\phi^{NP} - \phi^L]$, which differs from $E = \phi^R - \phi^L$, the experimentally accessible quantity. To estimate $[\phi^{NP} - \phi^L]$, it would be necessary to make new assumptions about surface potentials. If it were assumed, as has been proposed by Plieth [65], that the surface potential of MNPs in contact with the solution is similar to that of the massive metal in contact with the same electrolyte, one would obtain: $[\phi^{NP} - \phi^L] \approx [\psi^{NP} - \psi^L]$. This is a negative Galvani potential difference of quite large magnitude due to the work function difference. However, this conclusion is questionable. Note that Eq. 15 was derived on a purely thermodynamic basis and differs from that derived by Plieth [23], who assumed constant surface charge along the dispersion process, a speculation without supporting evidence. Our argument evidences that as the size of the MNPs becomes smaller the Volta potential, ψ^{NP}, of the metal decreases. Therefore, the charge distribution within the double-layer and consequently the surface potential should be affected. Consequently, the charge density of each particle will depend on its size, and therefore the surface tension of each particle will also depend on the size due to charge differences.

3.2. Thermodynamic Analysis of the Cell Potential for Polydisperse Ensembles of Nanoparticles

In this section, we will analyze some aspects of our thermodynamic approach and its applicability for actual ensembles of supported MNPs.

First, it is noticeable that Eq. 8 reduces to Eq. 1 for a monodisperse system, a proof of consistency that is not verified in the paper by Brainina et al. [41]. Moreover Eq. 8 shows that higher moments of the probability distributions become of interest, as well as the mean values. It is remarkable that, in the same way that the entropy of a whole ensemble of particles (see Eqs. 1-6 in Ref. [39]) is a property of the complete probability distribution, the redox potential is not simply "an average", but a characteristic of the collection, which requires a set of statistic variables for a reasonable description. In other words, the redox potential should be seen as a property of the whole probability distribution, rather than as a simple average quantity.

Second, it is interesting to estimate the magnitude of the deviation predicted by Eq. 8, if applicable, with respect to the potential of a bulk electrode and also in comparison to a monodisperse system. To do so, we will consider Ag NPs with normal distribution of their number of atoms, N, as in Section 2.1. The appropriate choice of $\bar{N}$ and σ_N ($\bar{N} = 6949$; $\sigma_N = 4090$) leads to common values of $\bar{d}$ and σ; which resulted 6.0 and 1.2 nm, respectively (i.e., the variation coefficient $\varepsilon = \sigma/\bar{d} = 1/5$). We have chosen these statistical parameters after considering literature data representative of Ag NPs [12,17,66], which were prepared by a variety of synthesis routes. A strict definition of a monodisperse system is not useful for real samples. Note that standard deviations greater than 15% of the mean were used [67]. Indeed, most of the methods for synthesizing MNPs lead to size distributions whose relative dispersions are greater than 20% [12,68–72]. In particular, dodecanethiolate-protected Au and Pd nanoparticles prepared by the Brust-Shiffrin two-phase method have shown dispersions of 24% (ε=0.24) [73] and 27% (ε=0.27) [74], respectively.

For Ag NPs of $\bar{d} = 6.0\ nm$ and $\sigma = 1.2nm$ Eq. 8 predicts an $E = -0.104\ V\ vs.\ E_{Ag^+/Ag^0}^{bulk}$, a considerable magnitude. On the other hand, the potential shift for a monodisperse set of Ag NPs of 6.0 nm (Eq. 1 or $\sigma_N = 0$ in Eq. 8) is -0.092 V. Therefore, for this typical situation, the broadness of the distribution strongly affects the contribution from surface effects, which manifests as a 13% augmented potential shift. It is remarkable that, for both systems, the predicted potential shift is negative enough to induce Ag^+ deposition onto the inert electrode. Whether new nanoparticles (or nuclei) could form or just electrochemical Ostwald ripening would occur, will depend on the nucleation overpotential.

There are a couple of issues regarding the purely thermodynamic approach. First of all, to obtain $\mu_{(T,p,\bar{N},\sigma)}$ the derivative with respect to $\bar{N}$ has been done while keeping the other variables as constants. This mathematical operation is possible for the normal distribution, but cannot be carried out for most size-distributions. For instance, the mean value of a log-normal distribution depends both on the median and the standard deviation of the variable's natural logarithm (see SI, section S2, Eq. S17). This drawback is also found for other probability distribution functions [75]. Secondly, there is another point that has to be considered. We should reconsider the restriction of N constant, which implies that every small system is closed. A Au nanoparticle made up of N atoms in an inert electrolyte is a clear-cut example, which could be analyzed as an ideally polarizable electrode. But an aggregate of metal atoms able to be oxidized and/or experience an electrochemical deposition would be open rather than closed. The criterion distinguishing the two cases is whether or not the system maintains N = constant, within experimental error, during the time required for the thermodynamic measurement of interest. However, it can be clearly seen that the present approach would fail to describe actual ensembles of reactive MNPs. This is the case, for instance, of Ag NPs in contact with an electrolyte

containing silver cations. If particles of significantly different size were subjected to the same redox potential, net electrochemical reactions would be experienced by most of these nanoparticles, which is usually described as electrochemical Ostwald ripening [76]. It seems that the model which maintains N = constant would not successfully describe highly reactive systems, as those with high exchange current densities, which are similar to ideally non-polarizable electrodes. Therefore, in the next section we analyze our alternative model, which is based on electrochemical kinetics concepts and on the mixed potential formalism.

3.3 The Redox Potential as a Mixed Potential.

In section 2.2 we derived Eq.14, which allows the calculation of $E_{mix(\bar{d},\sigma)}$ for a MNPs'-size distribution of any shape. In this section we will concentrate on the analysis of this equation for different situations, and we will also compare our results to those in previous reports [40]. Now, we will consider some limiting cases in order to prove that Eq. 14 is qualitatively suitable to describe MNPs ensembles in different hypothetical situations. For the sake of simplicity, it is assumed that the $\Delta\mu_{(d)}$ can be expressed according to the Gibbs-Thompson equation. First, if a monodisperse system is considered, Eq. 14 reduces to Eq. 1. Second, let's consider relatively large nanoparticles (sizes of a few tens of nanometers), i.e. for which $\Delta\mu_{(d_k)} \ll RT$. This allows the linearization of the exponentials in Eq. 14 leading to:

$$E_{mix(\bar{d},\sigma)} = E_{M^{z+}/M^0}^{bulk} - \frac{4\gamma V_m}{zF}\frac{\sum_k d_k}{\sum_k d_k^2} \qquad [17]$$

Note that the Eq. 17 is equivalent to the Eq. 8 in the paper by Schröder et al. [40]. However, as we will show below, it is not suitable for the analysis of actual samples of MNPs, unless they were all large enough. Nonetheless, this equation has additional consequences, which can be unveiled by expressing it in terms of $\bar{d}$ and σ:

23

$$E_{mix(\bar{d},\sigma)} = E^{bulk}_{M^{z+}/M^0} - \frac{4\gamma V_m}{ZF\bar{d}}\left[\frac{1}{1+(\sigma/\bar{d})^2}\right] \qquad [18]$$

Notably, $E_{mix(\bar{d},\sigma)}$, the quantity which is experimentally accessible through *ocp* measurements, depends on both statistical parameters, $\bar{d}$ and σ. Moreover, the
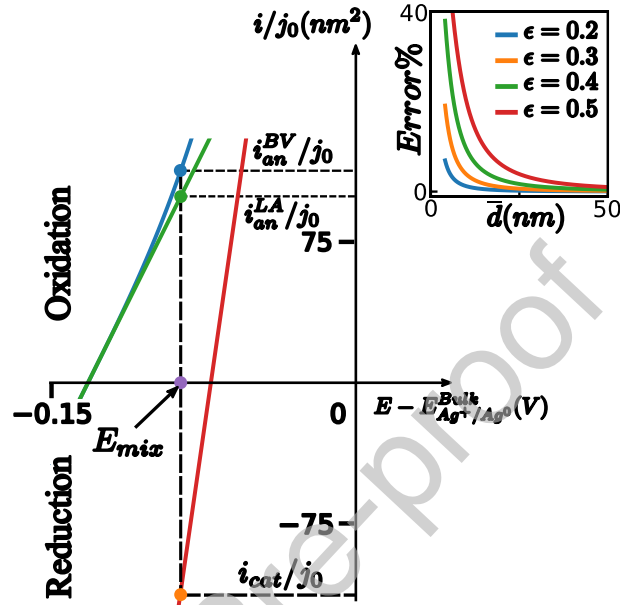

Figure 2. i/j_0 vs. potential curves for a two-particle system. The Ag particles have $\bar{d}$=5.0 nm and $\varepsilon = 0.3$. For the smaller NP $(d = 4.2\ nm)$ i^{BV}_{an}/j_0 is represented in light blue, and i^{LA}_{an}/j_0 as a green line. For the larger one, $(d = 7.8\ nm)$, just the linear approach is drawn (red line). The right panel shows the dependence of the relative error, $Error\% = (|i^{BV}_{an} - i^{LA}_{an}|/i^{BV}_{an}).100$, with $\bar{d}$ for different values of ε.

convenience of the definition of the variation coefficient, $\varepsilon = \sigma/\bar{d}$, to describe electrochemical systems is clearly seen. However, the most relevant aspect of Eq. 18 is that it predicts a decrease in the net effect of the excess surface free energy when the size dispersion becomes wider. However, Eqs. 17 and 18 are approximations which fail to predict precisely E_{mix} when small MNPs are present. If this were the case, the linearization of the exponentials in Eqs. 13 and 14, which originates in the Butler-Volmer equation, would not be correct. To illustrate it, Fig. 2 compares the oxidation current predicted by the Butler-Volmer equation, i^{BV}_{an}, with that for the linear approximation, i^{LA}_{an}. For convenience $1/j_0$ is used as a scaling factor. For $\bar{d}$ =5.0 nm and ε= 0.3, i^{BV}_{an}/j_0 and

24

i_{an}^{LA}/j_0 are quite different, although the mixed potentials calculated using these currents are similar due to error compensation. The situation gets worse as the sizes becomes smaller (see inset in Fig. 2). Therefore, the linear approach is not suitable to describe MNPs dispersions with significant contributions from particles smaller than 10 nm. This would be the case of Ostwald-ripening processes as those studied by Brus et al. [76].

3.4 The redox potential of metal nanoparticles in a dispersed state

Then, we study different log-normal size distributions of Ag NPs within the context of the mixed potential theory. To illustrate the most relevant aspects, panels a and b in Figure 3 show two log-normal size distributions, which only differ in their broadness. In Figure 3 (a) $\bar{d} = 6.0\ nm$ and $\sigma = 1.2 nm$, while in Figure 3.b $\bar{d} = 6.0\ nm$ and $\sigma = 3.0\ nm$. We consider, as before, Ag NPs and the Gibbs-Thompson equation to calculate $\Delta\mu_{(d)}$. Thus, for both size distributions, Eq. 14 allows the calculation of $E_{mix(\bar{d},\sigma)}$, which are represented by blue horizontal lines in Figure 3.c-d. As can be seen, the narrower distribution shows a lower $E_{mix(\bar{d},\sigma)}$ ($E_{mix(\bar{d}=6.0\ nm,\sigma=1.2\ nm)} = -0.091\ V$ vs. E_{M^{z+}/M^0}^{bulk}) than the wider one ($E_{mix(\bar{d}=6.0\ nm,\sigma=3.0\ nm)} = -0.077\ V$ vs. E_{M^{z+}/M^0}^{bulk}). Note that both figures are above the value for a monodisperse system ($E_{(\bar{d}=6.0\ nm,\sigma=0.0\ nm)} = -0.092\ V$, Eq. 1). In these panels the electrode potentials are represented on the right axes, and the green curves represent the behavior predicted by Plieth for monodisperse systems (Eq. 1). The respective $E_{mix(\bar{d},\sigma)}$ match those expected for particles of certain equivalent diameters, $d_{eq(\bar{d},\sigma)}$, which are indicated by the vertical blue lines. It means that if particles of these sizes were immersed in media with $E_{mix(\bar{d},\sigma)}$, these $E_{mix(\bar{d},\sigma)}$ would be coincident with their respective equilibrium potentials, $E_{(d_{eq(\bar{d},\sigma)})}$. Notably, for both
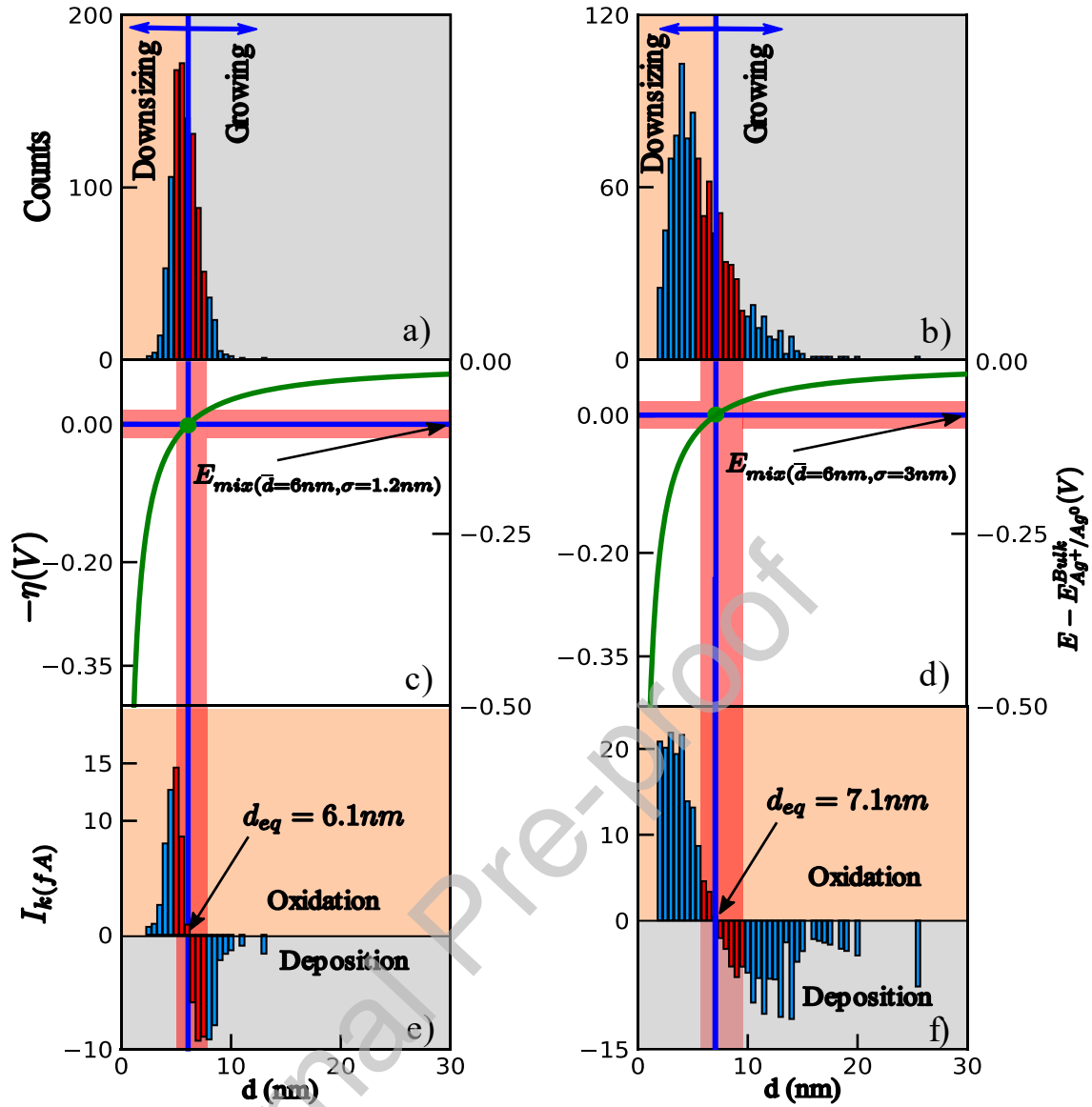
Figure 3. (a-b) Two simulated log-normal size distributions: (a), $\bar{d} = 6.0\ nm$; $\varepsilon = 0.2$. (b) $\bar{d} = 6.0\ nm$; $\varepsilon = 0.5$. Panels (c) and (d) show the $E\ vs.\ d$ according to the model by Plieth as a solid green line. The E_{mix} from (a) and (b) are represented as horizontal lines in (c) and (d), respectively. $E\text{-}E_{M^{z+}/M^0}^{bulk}$ are shown in the right axes, while overpotentials are shown in the left ones. The green points and vertical lines mark the equivalent diameters, $d_{eq(\bar{d},\sigma)}$. Panels (e) and (f) show the current contribution for each class of NP. The red bars and pink shading show the regions where the linearized Butler-Volmer equation is applicable.

size distributions shown in Figure 3, $d_{eq(\bar{d},\sigma)} > \bar{d}$. The particles with sizes smaller than $d_{eq(\bar{d},\sigma)}$ will tend to oxidize, since they are dispersed in a media with a redox potential higher than their equilibrium potential, $E_{(d_k)}$. On the contrary, particles bigger than $d_{eq(\bar{d},\sigma)}$ will tend to grow at the expense of the smaller-ones. The above-described oxidation-reduction processes lead to the well-documented electrochemical Ostwald ripening, which will be analyzed in more detail below.

First, we can see that $E_{mix(\bar{d},\sigma)} = E_{(d_{eq(\bar{d},\sigma)})}$ leads to the definition of the overpotentials, $\eta_{(d_k)} = E_{mix(\bar{d},\sigma)} - E_{(d_k)}$ (left axes in Figure 3.c-d), which are necessary for the calculation of the current density of a particle, according to Eq. 12. Note that the $\eta_{(d_k)} = 0$ condition corresponds to different situations depending on the $E_{mix(\bar{d},\sigma)}$ values. Then, the current associated to each particle size can be calculated according to: $i_{(d_k)} = 4\pi d_k^2 . j_{k(d_k; E_{mix(\bar{d},\sigma)})}$. The $i_{(d_k)}$s calculated for the size-distributions in Figure 3.a-b are shown, respectively, in panels e and f. It is interesting to note that the current contribution of the less abundant particles -i.e. those with too small sizes or sizes more than twice $\bar{d}$- is more important than that from those particles near $d_{eq(\bar{d},\sigma)}$. The origin of this behavior can be explained by considering the exponential dependences of the oxidation and reduction terms in Eq. 12. For d_k relatively far from $d_{eq(\bar{d},\sigma)}$, $E_{(d_k)}$ significantly differs from $E_{mix(\bar{d},\sigma)}$ leading to great absolute values of the current density. This result anticipates that the linear approach to the Butler-Volmer equation will seriously underestimate the absolute values of the current densities. Then, we discriminate the sizes for which the linear approach leads to estimates of the current with errors of less than 2.5% [61], which are represented as red bars in Figure 3.a,b,e,f, and define the pink-shadow regions in panels c and d. Note that, even for the narrowest distribution, the linear approach does not take into account most of the current contributions (bars in light-blue in Figure 3.a,b,e,f). Moreover, the number of particles that require the use of the Butler-Volmer equation as it is, increases as the broadness of the distribution does. In fact, as mentioned above, the particles outside the central region contribute the most to the current (Figure 3.e-f), so they would be determining for the ripening processes. The smaller MNPs have a significant population and they have a great tendency to oxidation, due to the exponential factor, $e^{-\alpha f E_{(d_k)}/RT}$ in the Butler-Volmer

equation. On the other hand, in addition to the effect of $E_{(d_k)}$, as a factor $e^{(1-\alpha)fE_{(d_k)}}$, the increase in area plays a determining role in the deposition process for larger particles. Although the above discussion was based in the analysis of log-normally distributed sizes, equivalent results can be found for normal size distributions (see SI). Thus, we can conclude that the linear approximation would not be suitable for the estimation of the $E_{mix(\bar{d},\sigma)}$. Furthermore, it is definitively useless to account for the currents; and therefore, it is not suitable to describe the electrochemical Ostwald ripening processes.

Next, we will estimate the time required for the complete oxidation of a 3 nm Ag NP belonging to the size distribution of Figure 3.a. By the application of Eq. 12, and using $E_{mix(\bar{d},\sigma)} = -0.091\ V$, the instantaneous net current for this single particle results 0.23 fA (2.3x10^{-16} A). If this current were to hold steady for the lifetime of the particles, even if their size changed, it would disappear after about 1 second. However, real dispersions of MNPs can be stored for long time periods. Therefore, the above estimation overestimates the reactivity of MNPs. The j_0 employed, which is representative of clean Ag surfaces (i.e., not blocked by strongly adsorbing species), is probably orders of magnitude greater than that expected for nanoparticles protected by common capping agents. These adsorbates not only modify the surface tension, they also strongly hinder the electrochemical processes related with electrochemical Ostwald ripening as stated by Brus [76]. Furthermore, the capping agents can substantially influence the reactivity. While neutral adsorbates change the surface potential, ionic species also modify the surface charge [32]. Despite this apparent limitation, the present model could successfully describe the electrochemical behavior of a set of MNPs if appropriate j_0s values are used. As a suitable approximation, these data could be obtained from polarization curves of bulk electrodes covered by the corresponding capping agents.

3.5 Comparison of the Thermodynamic and Electrochemical Kinetic Models

Now we will compare the results from the purely thermodynamic approach to those derived from electrochemical concepts. To do so, we have calculated the E values according to the thermodynamic model, Eq. 8, and also by means to the electrochemical kinetic model, Eq. 14, for a series of Gaussian size-distributions of Ag NPs, all of which have the same $\bar{d}$=6.0 nm, but different broadness. We have chosen the appropriate sets $(\bar{N}, \sigma_N)$ -$\bar{N}$ and σ_N characterize the normal distributions to be considered-, which allow the evaluation of E for a variety of ε values, while maintaining $\bar{d}$ constant. Notably, a normal distribution in N leads to a negatively skewed size distribution, as it is illustrated in the inset in the bottom half of Figure 4. As predicted by Eq. 8, the contribution from the surface free energy increases as the broadness of the distribution does, which is evident in the decaying behavior of the E vs. ε curve. On the contrary, the electrochemical model predicts an increase in the redox potential as the distribution becomes wider. This behavior, which is opposite in relation with the thermodynamic model, is verified for every distribution shape. Although the tendencies are opposite, both models converge to the same E for a monodisperse system, which represents a strong test of consistency. It is not surprising to find such diverging behaviors between the results from these models

since they were developed on a completely different basis. While the thermodynamic approach is based on the idea that the MNPs are unreactive, the key statement in the derivation of the kinetic electrochemical model is a reactivity balance, which is expressed as a null-current condition. However, in both cases it is clear that not only the knowledge of the mean value of a size distribution is mandatory for a correct characterization of a system, but also its standard deviation, which strongly influences the operationally accessible properties.

At this point, it is necessary to review the implications of both models by considering their argumentation routes. First of all, a monodisperse ensemble of nanoparticles does not represent a system under thermodynamic equilibrium, since actual equilibrium would be attained when a bulk material is obtained. However, to ensure consistency it is still useful to compare the results from our models with those valid for monodisperse systems. Once proved that both models tend to the behavior of a
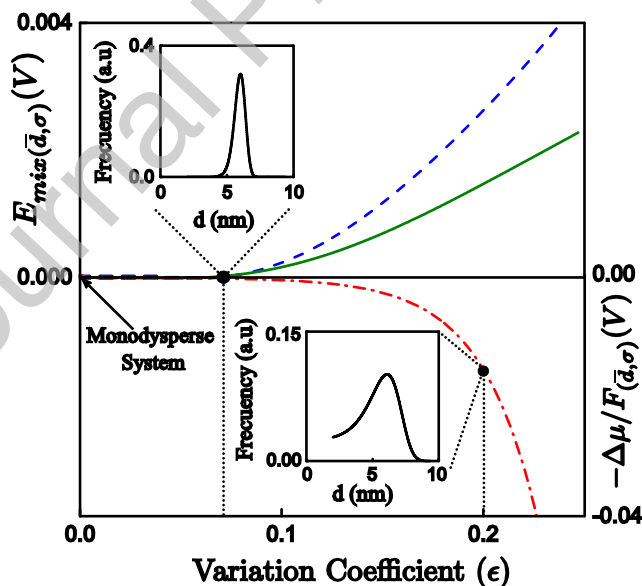

Figure 4. $E_{Mix(\bar{D},\sigma)}$ and $-\Delta\mu/F_{(\bar{D},\sigma)}$ as a function of ε for Ag nanoparticles ($\bar{d}$=6.0 nm), taking as reference the quantities for the monodisperse system: $E_{Mix(\bar{D},\sigma=0)}$ and $-\Delta\mu/F_{(\bar{D},\sigma=0)}$. The green and light blue curves correspond to the electrochemical kinetic model and the linearized Butler-Volmer equation, respectively. $-\dfrac{\Delta\mu_{poly}}{zF}$ vs. ε from the thermodynamic model is represented in red. Examples of the size distributions used for the calculations are shown in the insets.

monodisperse one, it is still challenging to explain why their tendencies are opposite when the broadness of the distribution increases.

In the case of the thermodynamic model the particles are kinetically trapped, since the unreactive constraint is imposed. Therefore, it is not guaranteed that they can lead to a well-established electrode potential. Under such boundary condition, Eq. 8 shows that the chemical potential of the ensemble increases as the size distribution becomes broader. On the other hand, the electrochemical kinetic model is based on the ability of the system to interchange charge between two phases, which unequivocally determines the electrode potential. Then, it shows increasingly higher redox potentials for broader size distributions. This does not mean that the electrochemical system has a lower tendency to MNPs' oxidation, but that its reactivity leads to the establishment of the null current condition at a higher potential. Incidentally, although the supported MNPs are far from thermodynamic equilibrium, the redox reactions allow the establishment of an experimentally measurable potential. Moreover, although the monodisperse system has lower free energy than the polydisperse one, the electrochemical pathway would not pass through the monodisperse situation on its way to the bulk material. On the contrary, it is expected that the smaller particles will disappear, in favor of the growth of the larger ones. This behavior has been widely accepted in descriptions of the electrochemical Ostwald ripening. Finally, rephrasing the question due to Plieth, we ask: What is the redox potential of an actual ensemble of metal nanoparticles? The answer is given by the electrochemical approach (Eq. 14) since the establishment of a redox potential requires charge-transfer among reacting entities. From there, the electrochemical system will evolve through a pathway that has to satisfy the null current boundary condition of the mixed potential theory. In this direction, the electrochemical kinetic model can straightforwardly be applied to theoretically study how the size distribution evolves,

together with the corresponding evolution of the mixed potential. Indeed, it would be useful to interpret the experimentally observed *ocp* evolution together with changes in size-distributions [77,78]. Also, it would be useful to quantitatively model the electrochemical Ostwald ripening under *ocp* conditions, considering that both E_{mix} and the size distribution will evolve [40]. This is quite different from models where a fixed electrode potential is applied, as those used to interpret the degradation of Pt NPs under harsh conditions [51,53], since no net metal dissolution is allowed at *ocp*.

On the other hand, the approach which considers the MNPs as inert entities would be valuable to evaluate the stability of the system on a thermodynamic basis. Indeed, if polydispersity were considered in thermodynamic cycles -as those described in the paper by Plieth-, our thermodynamic approach would be a suitable tool.

Finally, although for simplicity we have not carried out calculations including other contributions to the chemical potential of the MNPs, the electrochemical kinetic model can be straightforwardly applied to account for a variety of phenomena. Indeed, Eq. 14 is suitable to take into consideration the contributions from different crystal faces, an issue that has been pointed out in previous studies [20,51].

4.- Conclusions

In this work we have demonstrated that the redox potential of an ensemble of supported MNPs would be accessible through open circuit potential measurements. We have presented two approaches to calculate the cell potential for a polydisperse system. For both, the thermodynamic and the electrochemical kinetic model, the potential follows Nernstian behavior and depends on -at least- two statistical parameters, the average size and its variance. For a fixed average size, the thermodynamic model predicts an increase in the chemical potential of the metal as the size distribution becomes broader, leading to

a decrease in the electrode potential. In contrast, within the electrochemical kinetic model, broader distributions lead to higher electrode potentials. If this was not taken into account, the range of stability of the nanoparticles would be incorrectly estimated. However, this aspect is critical to assess the degradation of nanoparticles that undergo electrochemical Ostwald ripening.

Our electrochemical kinetic model can be extended to go beyond the Gibbs-Thompson equation, inasmuch it admits alternative expressions for the surface contribution to the chemical potential. Additionally, it is suitable for studying processes such as electrochemical Ostwald ripening, since it allows the calculation of the net current for each metallic-NP, irrespective of its size.

As expected from previous research on Ostwald ripening [79–83], our results indicate that the stability of a real sample of nanoparticles has to be studied by the thoughtful analysis of the rate of the oxidation and deposition processes of the whole set of particles, instead of simply analyzing the thermodynamic properties of a particle whose size is equal to the average.

References

[1]   Y. Mao, H. Zhang, S. Ahmed, S. Li, S. Zhang, J. Wang, Efficient and continuous chemical conversion in a thin membrane comprising three-dimensional network trapping Ag nanoparticles, Appl. Catal. B Environ. 314 (2022) 121456. https://doi.org/10.1016/j.apcatb.2022.121456.

[2]   J. Jiang, S. Yang, W. Wei, S. Tu, X. Zheng, L. Ai, Rational design of Ni

nanoparticles loaded porous N-doped carbon nanostructures for efficient

hydrogenation reduction of Cr(VI): Performance, critical role of hydrogen

species and mechanism insight, Appl. Surf. Sci. 625 (2023) 157170.

https://doi.org/10.1016/j.apsusc.2023.157170.

[3]   L. Abad-Gil, C.M.A. Brett, Poly(methylene blue)-ternary deep eutectic

solvent/Au nanoparticle modified electrodes as novel electrochemical sensors:

Optimization, characterization and application, Electrochim. Acta. 434 (2022)

141295. https://doi.org/10.1016/j.electacta.2022.141295.

[4]   Z. Li, Q. Fu, Y. Xue, Z. Cui, Effect of size on dissolution thermodynamics of

nanoparticles: A theoretical and experimental research, Mater. Chem. Phys. 214

(2018) 499–506. https://doi.org/10.1016/j.matchemphys.2018.04.112.

[5]   R.W. Murray, Nanoelectrochemistry: Metal Nanoparticles, Nanoelectrodes, and

Nanopores, Chem. Rev. 108 (2008) 2688–2720.

https://doi.org/10.1021/cr068077e.

[6]   B. Molleman, T. Hiemstra, Time, pH, and size dependency of silver nanoparticle

dissolution: the road to equilibrium, Environ. Sci. Nano. 4 (2017) 1314–1327.

https://doi.org/10.1039/C6EN00564K.

[7]   E. Kolle-Görgen, G. Fortunato, M. Ledendecker, Catalyst Stability in Aqueous

Electrochemistry, Chem. Mater. 34 (2022) 10223–10236.

https://doi.org/10.1021/acs.chemmater.2c02443.

[8]   G.D.M.R. Dabera, M. Walker, A.M. Sanchez, H.J. Pereira, R. Beanland, R.A.

Hatton, Retarding oxidation of copper nanoparticles without electrical isolation

and the size dependence of work function, Nat. Commun. 8 (2017) 1894.

https://doi.org/10.1038/s41467-017-01735-6.

[9]   E. Zhu, M. Wu, H. Xu, B. Peng, Z. Liu, Y. Huang, Y. Li, Stability of Platinum-
       Group-Metal-Based Electrocatalysts in Proton Exchange Membrane Fuel Cells,
       Adv. Funct. Mater. 32 (2022) 2203883. https://doi.org/10.1002/adfm.202203883.

[10]   K. Sieradzki, R.C. Cammarata, X. Li, L. Tang, C. Friesen, Electrochemical
       Stability of Elemental Metal Nanoparticles, J. Am. Chem. Soc. 132 (2010)
       11722–11726. https://doi.org/10.1021/ja104421t.

[11]   L. Tang, B. Han, K. Persson, C. Friesen, T. He, K. Sieradzki, G. Ceder,
       Electrochemical Stability of Nanometer-Scale Pt Particles in Acidic
       Environments, J. Am. Chem. Soc. 132 (2010) 596–600.
       https://doi.org/10.1021/ja9071496.

[12]   Olga S. Ivanova, Francis P. Zamborini, Size – Dependent Electrochemical
       Oxidation of Silver Nanoparticles, J. Am. Chem. Soc. 132 (2010) 70–72.
       https://doi.org/10.1021/ja908780g.

[13]   H.S. Toh, C. Batchelor-McAuley, K. Tschulik, M. Uhlemann, A. Crossley, R.G.
       Compton, The anodic stripping voltammetry of nanoparticles: Electrochemical
       evidence for the surface agglomeration of silver nanoparticles, Nanoscale. 5
       (2013) 4884–4893. https://doi.org/10.1039/c3nr00898c.

[14]   D.K. Pattadar, F.P. Zamborini, Size Stability Study of Catalytically Active Sub-2
       nm Diameter Gold Nanoparticles Synthesized with Weak Stabilizers, J. Am.
       Chem. Soc. 140 (2018) 14126–14133. https://doi.org/10.1021/jacs.8b06830.

[15]   R.A. Masitas, I. V. Khachian, B.L. Bill, F.P. Zamborini, Effect of surface charge
       and electrode material on the size-dependent oxidation of surface-attached metal

nanoparticles, Langmuir. 30 (2014) 13075–13084.

https://doi.org/10.1021/la5029614.

[16]   O.S. Ivanova, F.P. Zamborini, Electrochemical size discrimination of gold

nanoparticles attached to glass/indium-tin-oxide electrodes by oxidation in

bromide-containing electrolyte, Anal. Chem. 82 (2010) 5844–5850.

https://doi.org/10.1021/ac101021q.

[17]   C.C.M. Neumann, C. Batchelor-McAuley, K. Tschulik, H.S. Toh, P. Shumbul, J.

Pillay, R. Tshikhudo, R.G. Compton, The surface energy of single nanoparticles

probed via anodic stripping voltammetry, ChemElectroChem. 1 (2014) 87–89.

https://doi.org/10.1002/celc.201300062.

[18]   Y. Yunfeng, X. Yongqiang, C. Zixiang, Z. Miaozhi, Effect of particle size on

electrode potential and thermodynamics of nanoparticles electrode in theory and

experiment, Electrochim. Acta. 136 (2014) 565–571.

https://doi.org/10.1016/j.electacta.2014.05.067.

[19]   H. Duan, Z. Cheng, Y. Xue, Z. Cui, M. Yang, S. Wang, Influences of nano-effect

on electrochemical thermodynamics of metal nanoparticles electrodes, J.

Electroanal. Chem. 882 (2021) 115037.

https://doi.org/10.1016/j.jelechem.2021.115037.

[20]   C. Wang, Z. Cui, Y. Xue, Y. Wang, M. Wang, B. Ji, J. Chen, Y. Xue, L. Zhang,

Theoretical and experimental studies on the size- and morphology-dependent

thermodynamics of nanoparticle electrodes, Thermochim. Acta. 708 (2022)

179140. https://doi.org/10.1016/j.tca.2021.179140.

[21]   M. Wang, Z. Cui, Y. Xue, A. Yan, X. Yu, X. Song, H. Li, Preparation of Nano-

bismuth with Different Particle Sizes and the Size Dependent Electrochemical

Thermodynamics, Electroanalysis. 31 (2019) 1316–1323.

https://doi.org/10.1002/elan.201800870.

[22] H. Duan, Z. Cui, Y. Xue, Q. Fu, X. Chen, R. Zhang, Determination Method and Size Dependence of Interfacial Tension between Nanoparticles and a Solution, Langmuir. 34 (2018) 8792–8797. https://doi.org/10.1021/acs.langmuir.8b01702.

[23] W.J. Plieth, Electrochemical Properties of Small Metal Clusters, J. Phys. Chem. 86 (1982) 3166–3170. https://doi.org/10.1021/j100213a020.

[24] O. Varnavski, G. Ramakrishna, J. Kim, D. Lee, T. Goodson, Critical Size for the Observation of Quantum Confinement in Optically Excited Gold Clusters, J. Am. Chem. Soc. 132 (2010) 16–17. https://doi.org/10.1021/ja907984r.

[25] C.M. Aikens, Electronic Structure of Ligand-Passivated Gold and Silver Nanoclusters, J. Phys. Chem. Lett. 2 (2011) 99–104. https://doi.org/10.1021/jz101499g.

[26] W. Schmickler, E. Leiva, A note on the surface stress and tension of solid metal electrodes, J. Electroanal. Chem. 453 (1998) 61–67. https://doi.org/10.1016/S0022-0728(98)00133-8.

[27] J. Lipkowski, W. Schmickler, D.. Kolb, R. Parsons, Comments on the thermodynamics of solid electrodes, J. Electroanal. Chem. 452 (1998) 193–197. https://doi.org/10.1016/S0022-0728(98)00136-3.

[28] Z. Yao, S. Wu, R. Padilla Silvas, N. Khichoomian, Z.A. Carrillo, S. Anz, P. Sun, Potentiometric Study of the Growth of a Single Au Nanoparticle, Electroanalysis. 35 (2023). https://doi.org/10.1002/elan.202200166.

[29] M. Valvo, Y.-C. Chien, A. Liivat, C.-W. Tai, Detecting voltage shifts and charge

storage anomalies by iron nanoparticles in three-electrode cells based on converted iron oxide and lithium iron phosphate, Electrochim. Acta. 440 (2023) 141747. https://doi.org/10.1016/j.electacta.2022.141747.

[30] F. Chassagneux, N. Couzon, C. Place, M. Maillard, A. Brioude, L. Bois, Electrochemical Properties of Silver Nanoparticles in Mesoporous Silica and Titania Films: Specific Behavior of Titania Composite, Langmuir. 39 (2023) 7317–7327. https://doi.org/10.1021/acs.langmuir.3c00334.

[31] P. Saha, D. Henckel, F. Intia, L. Hu, T. Van Cleve, K.C. Neyerlin, Anolyte Enhances Catalyst Utilization and Ion Transport Inside a CO_2 Electrolyzer Cathode, J. Electrochem. Soc. 170 (2023) 014505. https://doi.org/10.1149/1945-7111/acb01d.

[32] M.D. Scanlon, P. Peljo, M.A. Méndez, E. Smirnov, H.H. Girault, Charging and discharging at the nanoscale: Fermi level equilibration of metallic nanoparticles, Chem. Sci. 6 (2015) 2705–2720. https://doi.org/10.1039/c5sc00461f.

[33] D.K. Lee, S. Il Park, J.K. Lee, N.M. Hwang, A theoretical model for digestive ripening, Acta Mater. 55 (2007) 5281–5288. https://doi.org/10.1016/j.actamat.2007.05.048.

[34] A.J. Bard, L.R. Faulkner, Electrochemical Methods: Fundamentals and Applications, 2nd ed., Wiley, 2000.

[35] B. Luigjes, S.M.C. Woudenberg, R. de Groot, J.D. Meeldijk, H.M. Torres Galvis, K.P. de Jong, A.P. Philipse, B.H. Erné, Diverging Geometric and Magnetic Size Distributions of Iron Oxide Nanocrystals, J. Phys. Chem. C. 115 (2011) 14598–14605. https://doi.org/10.1021/jp203373f.

[36]   W. Xu-Fei, S. Li-Qun, Polydispersity effects on the magnetization of diluted

         ferrofluids: a lognormal analysis, Chinese Phys. B. 19 (2010) 107502.

         https://doi.org/10.1088/1674-1056/19/10/107502.

[37]   P. Letellier, M. Turmine, Displacement of voltammetric peaks with nanoparticles

         size: A nonextensive thermodynamic approach, Electrochim. Acta. 127 (2014)

         384–389. https://doi.org/10.1016/j.electacta.2014.02.041.

[38]   P. Letellier, A. Mayaffre, M. Turmine, Redox behavior of nanoparticules:

         Nonextensive thermodynamics approach, J. Phys. Chem. C. 112 (2008) 12116–

         12121. https://doi.org/10.1021/jp801040u.

[39]   T.L. Hill, Thermodynamics of Small Systems, J. Chem. Phys. 36 (1962) 3182–

         3197. https://doi.org/10.1063/1.1732447.

[40]   A. Schröder, J. Fleig, D. Gryaznov, J. Maier, W. Sitte, Quantitative Model of

         Electrochemical Ostwald Ripening and Its Application to the Time-Dependent

         Electrode Potential of Nanocrystalline Metals, J. Phys. Chem. B. 110 (2006)

         12274–12280. https://doi.org/10.1021/jp060788t.

[41]   K.Z. Brainina, L.G. Galperin, E. V. Vikulova, A.L. Galperin, The effect of the

         system polydispersity on voltammograms of nanoparticles electrooxidation, J.

         Solid State Electrochem. 17 (2013) 43–53. https://doi.org/10.1007/s10008-012-

         1852-y.

[42]   D. Gray, A. Cahill, Theoretical Analysis of Mixed Potentials, J. Electrochem.

         Soc. 116 (1969) 443. https://doi.org/10.1149/1.2411894.

[43]   The Theory of Transformations in Metals and Alloys, Elsevier, 2002.

         https://doi.org/10.1016/B978-0-08-044019-4.X5000-4.

[44]   P. Bridgman, The Logic Of Modern Physics, The Macmillan Company, New

York, 1958.

[45]   O.A. Oviedo, C.F.A. Negre, M.M. Mariscal, C.G. Sánchez, E.P.M. Leiva,

Underpotential deposition on free nanoparticles: Its meaning and measurement,

Electrochem. Commun. 16 (2012) 1–5.

https://doi.org/10.1016/j.elecom.2011.12.013.

[46]   J.O. Bockris, S.U.M. Khan, Surface Electrochemistry, Springer US, Boston, MA,

1993. https://doi.org/10.1007/978-1-4615-3040-4.

[47]   R. Borah, S.W. Verbruggen, Effect of size distribution, skewness and roughness

on the optical properties of colloidal plasmonic nanoparticles, Colloids Surfaces

A Physicochem. Eng. Asp. 640 (2022) 128521.

https://doi.org/10.1016/j.colsurfa.2022.128521.

[48]   A. Schröder, J. Fleig, J. Maier, W. Sitte, Inherent emf relaxation of

electrochemical cells with nanocrystalline Ag electrodes, Electrochim. Acta. 51

(2006) 4176–4181. https://doi.org/10.1016/j.electacta.2005.11.048.

[49]   A. V. Virkar, Y. Zhou, Mechanism of Catalyst Degradation in Proton Exchange

Membrane Fuel Cells, J. Electrochem. Soc. 154 (2007) B540.

https://doi.org/10.1149/1.2722563.

[50]   R.M. Darling, J.P. Meyers, Kinetic Model of Platinum Dissolution in PEMFCs, J.

Electrochem. Soc. 150 (2003) A1523. https://doi.org/10.1149/1.1613669.

[51]   J. Zhu, S. Hu, Z. Zeng, W.-X. Li, First-principles investigation of

electrochemical dissolution of Pt nanoparticles and kinetic simulation, J. Chem.

Phys. 151 (2019) 234711. https://doi.org/10.1063/1.5129631.

[52]   E. Budevski, G. Staikov, W.J. Lorenz, Electrochemical Phase Formation and

       Growth, Wiley, 1996. https://doi.org/10.1002/9783527614936.

[53]   G. Bucci, K. Gadelrab, W.C. Carter, Mesoscale Model for Ostwald Ripening of

       Catalyst Nanoparticles, J. Electrochem. Soc. 168 (2021) 054515.

       https://doi.org/10.1149/1945-7111/abf970.

[54]   C.L. Kuo, K.C. Hwang, Does morphology of a metal nanoparticle play a role in

       Ostwald ripening processes?, Chem. Mater. 25 (2013) 365–371.

       https://doi.org/10.1021/cm3031279.

[55]   A. Molina, J. Gonzalez, E.O. Barnes, R.G. Compton, Simple Analytical

       Equations for the Current–Potential Curves at Microelectrodes: A Universal

       Approach, J. Phys. Chem. C. 118 (2014) 346–356.

       https://doi.org/10.1021/jp409167m.

[56]   P.A. Bobbert, M.M. Wind, J. Vlieger, Diffusion to a slowly growing truncated

       sphere on a substrate, Phys. A Stat. Mech. Its Appl. 141 (1987) 58–72.

       https://doi.org/10.1016/0378-4371(87)90261-5.

[57]   J.H. Park, H. Zhou, S.J. Percival, B. Zhang, F.R.F. Fan, A.J. Bard, Open circuit

       (mixed) potential changes upon contact between different inert electrodes-size

       and kinetic effects, Anal. Chem. 85 (2013) 964–970.

       https://doi.org/10.1021/ac3025976.

[58]   H. Kawano, Effective Work Functions of the Elements, Prog. Surf. Sci. 97

       (2022) 100583. https://doi.org/10.1016/j.progsurf.2020.100583.

[59]   L. Zhou, M.R. Zachariah, Size resolved particle work function measurement of

       free nanoparticles: Aggregates vs. spheres, Chem. Phys. Lett. 525–526 (2012)

77–81. https://doi.org/10.1016/j.cplett.2011.11.045.

[60]   M. Seidl, K. -H. Meiwes-Broer, M. Brack, Finite-size effects in ionization

potentials and electron affinities of metal clusters, J. Chem. Phys. 95 (1991)

1295–1303. https://doi.org/10.1063/1.461111.

[61]   J.O. Bockris, A.K.N. Reddy, Gamboa-Aldeco, Modern Electrochemistry 2A,

Kluwer Academic Publishers, Boston, 2002. https://doi.org/10.1007/b113922.

[62]   A.F. Silva, ed., Trends in Interfacial Electrochemistry, Springer Netherlands,

Dordrecht, 1986. https://doi.org/10.1007/978-94-009-4694-1.

[63]   M. Schnippering, M. Carrara, A. Foelske, R. Kötz, D.J. Fermín, Electronic

properties of Ag nanoparticle arrays. A Kelvin probe and high resolution XPS

study, Phys. Chem. Chem. Phys. 9 (2007) 725–730.

https://doi.org/10.1039/b611496b.

[64]   A.L. Dadlani, P. Schindler, M. Logar, S.P. Walch, F.B. Prinz, Energy States of

Ligand Capped Ag Nanoparticles: Relating Surface Plasmon Resonance to Work

Function, J. Phys. Chem. C. 118 (2014) 24827–24832.

https://doi.org/10.1021/jp5073044.

[65]   W.J. Plieth, The work function of small metal particles and its relation to

electrochemical properties, Surf. Sci. 156 (1985) 530–535.

https://doi.org/10.1016/0039-6028(85)90615-6.

[66]   N.R. Jana, L. Gearheart, C.J. Murphy, Wet chemical synthesis of silver nanorods

and nanowires of controllable aspect ratio, Chem. Commun. (2001) 617–618.

https://doi.org/10.1039/b100521i.

[67]   Q. Zhang, J. Xie, Y. Yu, J.Y. Lee, Monodispersity control in the synthesis of

monometallic and bimetallic quasi-spherical gold and silver nanoparticles, Nanoscale. 2 (2010) 1962–1975. https://doi.org/10.1039/c0nr00155d.

[68] M. Wuithschick, B. Paul, R. Bienert, A. Sarfraz, U. Vainio, M. Sztucki, R. Kraehnert, P. Strasser, K. Rademann, F. Emmerling, J. Polte, Size-controlled synthesis of colloidal silver nanoparticles based on mechanistic understanding, Chem. Mater. 25 (2013) 4679–4689. https://doi.org/10.1021/cm401851g.

[69] S. Chen, J.R. Drehmel, R.L. Penn, Facile Synthesis of Monodispersed Ag NPs in Ethylene Glycol Using Mixed Capping Agents, ACS Omega. 5 (2020) 6069–6073. https://doi.org/10.1021/acsomega.9b04492.

[70] N.G. Bastús, J. Piella, V. Puntes, Quantifying the Sensitivity of Multipolar (Dipolar, Quadrupolar, and Octapolar) Surface Plasmon Resonances in Silver Nanoparticles: The Effect of Size, Composition, and Surface Coating, Langmuir. 32 (2016) 290–300. https://doi.org/10.1021/acs.langmuir.5b03859.

[71] R. Ma, C. Levard, S.M. Marinakos, Y. Cheng, J. Liu, F.M. Michel, G.E. Brown, G. V. Lowry, Size-controlled dissolution of organic-coated silver nanoparticles, Environ. Sci. Technol. 46 (2012) 752–759. https://doi.org/10.1021/es201686j.

[72] L. Xing, Y. Xiahou, P. Zhang, W. Du, H. Xia, Size Control Synthesis of Monodisperse, Quasi-Spherical Silver Nanoparticles To Realize Surface-Enhanced Raman Scattering Uniformity and Reproducibility, ACS Appl. Mater. Interfaces. 11 (2019) 17637–17646. https://doi.org/10.1021/acsami.9b02052.

[73] J.C. Azcárate, S.A. Díaz, J.A. Fauerbach, F. Gillanders, A.A. Rubert, E.A. Jares-Erijman, T.M. Jovin, M.H. Fonticelli, ESIPT and FRET probes for monitoring nanoparticle polymer coating stability, Nanoscale. 9 (2017) 8647–8656. https://doi.org/10.1039/C7NR01787A.

[74] G. Corthey, A. Rubert, A. Picone, G. Casillas, L. Giovanetti, J. Ramallo-Lopez, E. Zelaya, G. Benitez, F. Requejo, M. José Yacamán, R. Salvarezza, M. Fonticelli, New Insights into the Chemistry of Thiolate-Protected Palladium Nanoparticles, J. Phys. Chem. C. 116 (n.d.) 9830–9837. https://doi.org/10.1021/jp301531n.

[75] G. c. Canavos, Applied probability and statistical methods, Little, Brown and Company, 1984.

[76] P.L. Redmond, A.J. Hallock, L.E. Brus, Electrochemical Ostwald ripening of colloidal Ag particles on conductive substrates, Nano Lett. 5 (2005) 131–135. https://doi.org/10.1021/nl048204r.

[77] E. V. Zolotukhina, T.A. Kravchenko, Synthesis and kinetics of growth of metal nanoparticles inside ion-exchange polymers, Electrochim. Acta. 56 (2011) 3597–3604. https://doi.org/10.1016/j.electacta.2010.12.019.

[78] P. Parthasarathy, A. V. Virkar, Electrochemical Ostwald ripening of Pt and Ag catalysts supported on carbon, J. Power Sources. 234 (2013) 82–90. https://doi.org/10.1016/j.jpowsour.2013.01.115.

[79] S. Hu, W. Li, Influence of Particle Size Distribution on Lifetime and Thermal Stability of Ostwald Ripening of Supported Particles, ChemCatChem. 10 (2018) 2900–2907. https://doi.org/10.1002/cctc.201800331.

[80] M. Iggland, M. Mazzotti, Population Balance Modeling with Size-Dependent Solubility: Ostwald Ripening, Cryst. Growth Des. 12 (2012) 1489–1500. https://doi.org/10.1021/cg201571n.

[81] A. Kregar, T. Katrašnik, Theoretical analysis of particle size re-distribution due

to Ostwald ripening in the fuel cell catalyst layer, Open Phys. 17 (2019) 779–789. https://doi.org/10.1515/phys-2019-0081.

[82] K. Wettergren, F.F. Schweinberger, D. Deiana, C.J. Ridge, A.S. Crampton, M.D. Rötzer, T.W. Hansen, V.P. Zhdanov, U. Heiz, C. Langhammer, High Sintering Resistance of Size-Selected Platinum Cluster Catalysts by Suppressed Ostwald Ripening, Nano Lett. 14 (2014) 5803–5809. https://doi.org/10.1021/nl502686u.

[83] D.K. Pattadar, F.P. Zamborini, Effect of Size, Coverage, and Dispersity on the Potential-Controlled Ostwald Ripening of Metal Nanoparticles, Langmuir. 35 (2019) 16416–16426. https://doi.org/10.1021/acs.langmuir.9b02421.

Credit Author Statement

Leonardo D. Robledo Candia: Investigation, Conceptualization, Methodology, Writing – original draft, Writing – review & editing.

Gabriel, C. Lavorato: Investigation, Conceptualization, review & editing.

Aldo A. Rubert: Investigation, Conceptualization, Supervision.

Mariano H. Fonticelli: Investigation, Conceptualization, Methodology, Supervision, Writing– original draft, Writing – review & editing, Funding acquisition.

Graphical Abstract
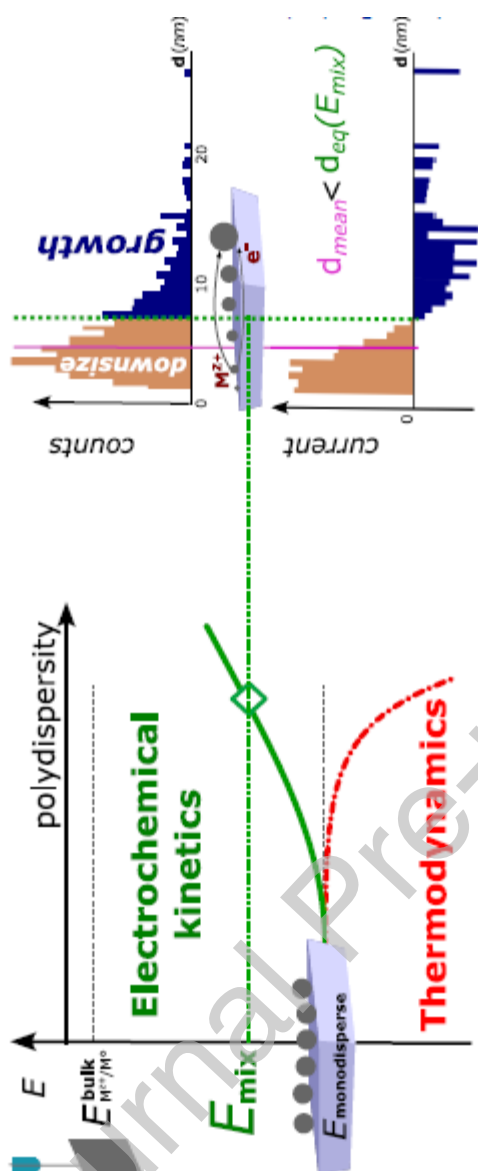
Declaration of interests

☒ The authors declare that they have no known competing financial interests or personal relationships that could have appeared to influence the work reported in this paper.

☐ The authors declare the following financial interests/personal relationships which may be considered as potential competing interests:

47